Original

Stepanek, M.; Skvarla, J.; Uchman, M.; Prochazka, K.; Angelov, B.;
Kovacik, L.; Haramus, V.M.; Mantzaridis, C.; Pispas, S.:

Wormlike core–shell nanoparticles formed by co-assembly of double hydrophilic block polyelectrolyte with oppositely charged fluorosurfactant

In: Soft Matter (2012) RSC Publishing

DOI: 10.1039/C2SM25588J

Soft Matter

Cite this: *Soft Matter*, 2012, **8**, 9412

www.rsc.org/softmatter

PAPER

Wormlike core–shell nanoparticles formed by co-assembly of double hydrophilic block polyelectrolyte with oppositely charged fluorosurfactant†

Miroslav Štěpánek,*[a] Juraj Škvarla,[a] Mariusz Uchman,[a] Karel Procházka,[a] Borislav Angelov,[b] Lubomír Kováčik,[c] Vasil M. Garamus,[d] Christos Mantzaridis[e] and Stergios Pispas*[e]

Received 14th March 2012, Accepted 4th May 2012
DOI: 10.1039/c2sm25588j

Formation of polyelectrolyte–surfactant complexes (PE–S) between an anionic polyelectrolyte, poly(sodium 2-sulfamate-3-carboxylate isoprene)-*block*-poly(ethylene oxide) (PSCI-PEO) and a cationic fluorosurfactant, *N*-(3,3,4,4,5,5,6,6,7,7,8,8,9,9,10,10,10-heptadecafluorodecyl) pyridinium chloride (HFDPCl) was studied in alkaline aqueous solutions by static, dynamic and electrophoretic light scattering. The structure of the formed PE–S nanoparticles was investigated by SAXS, cryogenic transmission electron microscopy and atomic force microscopy. The results show that the tendency of the fluorosurfactant to form elongated threadlike micelles drives the PE–S co-assembly to a flexible core–shell cylindrical morphology with the core of the PE–S and the shell of the PEO blocks. Unlike other PE–S systems involving double hydrophilic polyelectrolytes, well-defined core–shell particles exist only in the narrow range of HFDPCl-to-PSCI unit stoichiometric ratios corresponding to zero ζ-potential of the aggregates.

1 Introduction

Complexes of polyelectrolytes with oppositely charged surfactants (PE–S) have attracted the attention of many researchers in the past two decades due to the general interest in nanostructured self-assembled systems, as well as because of the pharmaceutical and other applications of these materials.[1–3] PE–S are stabilized by electrostatic interactions between the surfactant head groups and the polyelectrolyte side groups and by hydrophobic interactions between the hydrophobic backbone of the polyelectrolyte and the alkyl chains of the surfactant. It has been found that the oppositely charged surfactant condenses on the polyelectrolyte chains and forms micelles at concentrations far below its critical micelle concentration (cmc) in the absence of the polyelectrolyte[4,5] and that water-insoluble stoichiometric PE–S with zero net charge forms various water-insoluble ordered crystalline-like phases.[6]

Block copolymers consisting of a polyelectrolyte block and a neutral hydrophilic block (further referred to as double hydrophilic block polyelectrolytes, DHBE), such as poly(methacrylate)-*block*-poly(ethylene oxide)[7–9] or poly(acrylate)-*block*-poly(acrylamide)[10–12] co-assemble with oppositely charged ionic surfactants into core–shell particles with the shell formed by the neutral hydrophilic block and the core formed by the insoluble PE–S of the polyelectrolyte block and the surfactant. SANS and SAXS measurements indicate that the core contains disordered densely packed surfactant micelles.[10,11]

Surfactants with perfluorocarbon tails have been a subject of study due to their favorable properties, such as lower solubility in water, lower cmc and stronger surface activity compared with their hydrocarbon analogs.[13] Surfactants containing perfluorinated alkyl chains differ in many respects from hydrocarbon surfactants, not only because the fluorocarbon tail is both hydrophobic and lipophobic, but also because of its larger excluded volume compared with hydrocarbons, which causes fluorosurfactants to prefer self-assembly with a less curved interface, such as elongated micelles or vesicles.[13] Although a number of papers deal with complexes of homopolymers with fluorosurfactants[14–18] and the formation of co-assembled nanoparticles of block copolymers with fluorosurfactants in organic solvents has also been reported,[19,20] there are only a few studies on PE–S of DHBE with an oppositely charged fluorosurfactant in aqueous solutions.[21]

[a]*Department of Physical and Macromolecular Chemistry, Faculty of Science, Charles University in Prague, Hlavova 2030, 128 40 Prague 2, Czech Republic. E-mail: stepanek@natur.cuni.cz; Fax: +420 22499752; Tel: +420 221951292*
[b]*Institute of Macromolecular Chemistry, Academy of Sciences of the Czech Republic, Heyrovský Square 2, 16206 Prague 6, Czech Republic*
[c]*Institute of Cellular Biology, 1st Faculty of Medicine, Charles University in Prague, Albertov 4, 128 01 Prague 2, Czech Republic*
[d]*Helmholtz-Zentrum Geesthacht, Centre for Materials and Coastal Research, D-21502 Geesthacht, Germany*
[e]*Theoretical & Physical Chemistry Institute, National Hellenic Research Foundation, 48 Vassileos Constantinou Avenue, 11635 Athens, Greece. E-mail: pispas@eie.gr; Fax: +30 2107273824; Tel: +30 2107273794*
† Electronic supplementary information (ESI) available: (i) Zoomed views of objects on Cryo-TEM micrographs of a PSCI-PEO–HFDPCl system at $\beta = 0.71$ and (ii) the full expression for the scattering function $I_{PE-S}(q)$ (eqn (3)). See DOI: 10.1039/c2sm25588j

Here we report on the formation and structure of PE–S nanoparticles composed of an anionic DHBE, poly(sodium 2-sulfamate-3-carboxylate isoprene)-*block*-poly(ethylene oxide), PSCI-PEO,[22] and a cationic fluorosurfactant, *N*-(3,3,4,4,5,5,6,6,7,7,8,8,9,9,10,10,10-heptadecafluorodecyl) pyridinium chloride, HFDPCl, in alkaline aqueous solutions. It has been reported that, above a certain critical concentration (which is dependent on the ionic strength), HFDPCl undergoes a transition from spherical to elongated, threadlike micelles.[23] In this paper, we investigate how the tendency of the surfactant to form elongated micelles influences the co-assembly with DHBE. As a DHBE component of the studied PE–S complexes, we used PSCI-PEO, a biocompatible copolymer whose polyelectrolyte block contains both strong (SO_3H) and weak (COOH) acidic groups (similar to heparin[24,25]) and whose backbone is strongly hydrophobic due to the presence of unmodified poly(isoprene) units. The ability of PSCI-PEO to form nanoparticles with various positively charged species has been widely studied. It has been reported that PSCI-PEO copolymers form complexes with cationic polyelectrolytes and surfactants,[26] cationic vesicles,[27] proteins with a high isoelectric point[28] or bivalent metal cations.[29]

In this paper, the formation of PE–S between PSCI-PEO and HFDPCl is followed by a combination of static, dynamic and electrophoretic light scattering. The structure of the formed nanoparticles is studied in detail using small-angle X-ray scattering (SAXS), cryogenic transmission electron microscopy (Cryo-TEM) and atomic force microscopy (AFM).

2 Experimental

2.1 Materials

The PSCI-PEO copolymer (Fig. 1a) was prepared by the post-polymerization reaction of polyisoprene-*block*-poly(ethylene oxide) (PI-PEO), prepared by living anionic polymerization,[22] with chlorosulfonyl isocyanate. Details on the synthesis can be found in ref. 22. The weight average molar mass of the PI-PEO precursor by SEC was $M_w = 17.4$ kg mol^{-1}, and the PSCI-PEO sample composition by ^{13}C solid state NMR was 42, 34 and 24 mol% for the PEO units, PSCI units and unmodified polyisoprene units, respectively.

HFDPCl (Fig. 1b) was synthesized from 1*H*,1*H*,2*H*,2*H*-perfluorodecyl iodide and pyridine following the procedures outlined in ref. 30.

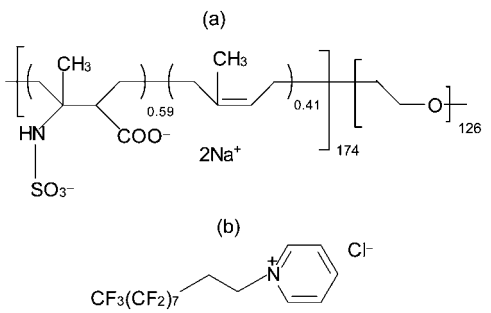

Fig. 1 Structures of (a) PSCI-PEO copolymer and (b) HFDPCl fluorosurfactant.

PE–S complexes were prepared by mixing stock solutions of PSCI-PEO and HFDPCl. Stock solutions of PSCI-PEO in 50 mM aqueous sodium tetraborate (pH 9.3) and HFDPCl in deionized water were mixed by stirring and left to stand for at least 24 hours for equilibration prior to the measurements. The PSCI-PEO concentration in the solutions was 1 mg mL^{-1}.

2.2 Methods

Static and dynamic light scattering measurements were carried out with an ALV photometer (ALV, Langen, Germany) consisting of a 22 mW He–Ne laser, an ALV CGS/8F goniometer, an ALV High QE APD detector and an ALV 5000/EPP multibit, multitau autocorrelator at 20 °C. The copolymer concentration in all the solutions was $c = 1$ mg mL^{-1}.

Static light scattering (SLS) measurements of the corrected excess scattering intensity $I(q)$ of the copolymer solutions, as a function of the magnitude of the scattering vector $q = (4\pi n_0/\lambda)\sin(\theta/2)$ (θ being the scattering angle, $n_0 = 1.332$ the refractive index of the solvent and $\lambda = 632.8$ nm the wavelength of the incident light) were treated by fitting the data in the angular range from 30° to 90° to the Guinier equation,

$$\ln \frac{I(q)}{I(0)} = -\frac{1}{3} R_g^2 q^2 \quad (1)$$

to obtain the forward scattering intensity, $I(0)$, and the radius of gyration, R_g.

Dynamic light scattering measurements were evaluated by fitting the measured normalized time autocorrelation function of the scattered light intensity, $g^{(2)}(t)$, related to the electric field autocorrelation function, $g^{(1)}(t)$, by the Siegert relation, $g^{(2)}(t) = 1 + \beta|g^{(1)}(t)|^2$, where β is the coherence factor. A constrained regularization algorithm (CONTIN) provided the distribution of relaxation times τ, $A(\tau)$, as the inverse Laplace transform of function $g^{(1)}(t)$

$$g^{(1)}(t) = \int_0^\infty A(\tau)\exp\left(-\frac{t}{\tau}\right)d\tau \quad (2)$$

The $A(\tau)$ distributions were recalculated to the distributions of apparent hydrodynamic radii, R_H^{app}, assuming the apparent diffusion coefficient $D^{app} = 1/\tau q^2$ and using the Stokes–Einstein formula, $R_H^{app} = k_B T/6\pi\eta D^{app}$, where k_B is the Boltzmann constant, T is the temperature and η is the solvent viscosity.

Electrophoretic light scattering measurements were carried out with a Nano-ZS Zetasizer (Malvern Instruments, UK). ζ-potential values were calculated from electrophoretic mobilities (averages of 15 to 100 measurements) using the Smoluchowski approximation.

SAXS experiments were performed on the P12 BioSAXS beamline at the PETRA III storage ring of the Deutsche Elektronen Synchrotron (DESY, Hamburg, Germany) at 20 °C using a Pilatus 2M detector and synchrotron radiation with a wavelength of $\lambda = 0.1$ nm. The sample-detector distance was 3 m, allowing for measurements in the q-range interval from 0.11 to 4.4 nm^{-1}. The q range was calibrated using the diffraction patterns of silver behenate. The experimental data were normalized to the incident beam intensity and corrected for non-homogeneous detector response, and the background scattering of the solvent was subtracted. The solvent scattering was

measured before and after the sample scattering to control for possible sample holder contamination. Eight consecutive frames comprising the measurement of the solvent, sample, and solvent were performed. No measurable radiation damage was detected by the comparison of eight successive time frames with 15 s exposures. The final scattering curve was obtained using the PRIMUS program by averaging the scattering data collected from the different frames. The automatic sample changer for sample volume 15 μL and filling cycle of 20 s was used.

Cryo-TEM measurements were carried out using a Tecnai G2 Sphera 20 electron microscope (FEI Company, Hillsboro, OR, USA) equipped with a Gatan 626 cryo-specimen holder (Gatan, Pleasanton, CA, USA). The samples for Cryo-TEM were prepared by plunge-freezing as described earlier.[31] Briefly, 3 μL of the sample solution was applied to an electron microscopy grid covered with perforated carbon supporting film (C-flat 2/2-2C, Electron Microscopy Sciences) glow discharged for 20 s with 5 mA current. Most of the sample was removed by blotting (Whatman no. 1 filter paper) for approximately 1 s, and the grid was immediately plunged into liquid ethane held at −183 °C. The grid was then transferred into the microscope without rewarming. Images were recorded at the accelerating voltage of 120 kV and microscope magnification ranging from 5000× to 14 500× using a Gatan UltraScan 1000 slow scan CCD camera (giving a final pixel size from 2 to 0.7 nm) and low dose mode with the electron dose not exceeding 1500 electrons per nm^2. Typical values of the applied underfocus ranged between 0.5 and 2 μm. The applied blotting conditions resulted in a specimen thickness varying between 100 to approx. 300 nm.

AFM measurements were performed in the tapping mode under ambient conditions using a commercial scanning probe microscope, Digital Instruments NanoScope dimensions 3, equipped with a Nanosensor silicon cantilever with a typical spring constant of 40 N m^{-1}. Polymeric micelles were deposited on a fresh (*i.e.*, freshly peeled out) mica surface (phlogopite, theoretical formula $KMg_3AlSi_3O_{10}(OH)_2$, from the Geological Collection of Charles University in Prague, Czech Republic) by a fast dip coating in a PSCI-PEO–HFDPCl aqueous solution (c approx. 10^{-2} g L^{-1}). After evaporation of the water, the sample was dried in a vacuum oven at ambient temperature for approx. 5 hours.

3 Results and discussion

3.1 Light scattering study of PE–S aggregate formation

First, the formation of PE–S in the PSCI-PEO–HFDPCl system was studied by static, dynamic and electrophoretic light scattering. Fig. 2 shows the dependences of the forward scattering intensity, $I(0)$ (curve 1) and the gyration radius, R_g (curve 2) of the PE–S aggregates formed in PSCI-PEO–HFDPCl alkaline aqueous solutions as functions of the stoichiometric ratio between the surfactant and the polyelectrolyte units of PSCI, β = [HFDPCl]/[SCI]. The results indicate that large aggregates are already present in a pure PSCI-PEO alkaline solution (R_g = 118 nm) due to hydrophobic interactions between unmodified isoprene units. For low β up to 0.36, both the average size of the scattering in the PSCI-PEO–HFDPCl solution and forward scattering intensity increase with the increasing

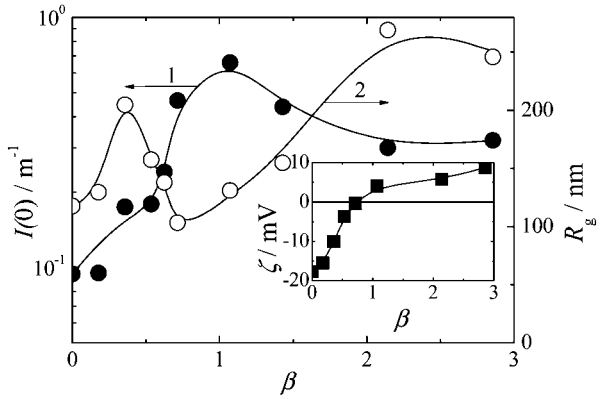

Fig. 2 Forward scattering intensity, $I(0)$ (curve 1), and gyration radius, R_g (curve 2) of PSCI-PEO–HFDPCl aggregates as functions of the stoichiometric ratio, β. Inset: ζ-potential of PSCI-PEO–HFDPCl aggregates as a function of β.

stoichiometric ratio as the formation of the PE–S complex further promotes the aggregation of PSCI-PEO chains. When the amount of the surfactant is further increased, R_g decreases (while $I(0)$ still grows) because the polyelectrolyte chains collapse due to charge neutralization by the bound surfactant micelles and consequent decrease in the electrostatic repulsion between the PSCI segments.

The above-mentioned charge neutralization can be followed by electrophoretic light scattering measurements. The inset in Fig. 2 shows the ζ-potential of the PSCI-PEO–HFDPCl system, which reflects the effective net charge of the formed PE–S aggregates as a function of β. The ζ values increase from negative to positive as an increasing amount of cationic surfactant is bound to the complex with the polyelectrolyte. The zero ζ-potential (and thus the zero effective charge of the PE–S nanoparticles) appears at $\beta = 0.71$, very close to the composition at which the gyration radius of the particles reaches its minimum value. On the other hand, the zero effective charge indicated by the ζ-potential measurement is attained at a much lower amount of the added surfactant than that expected from the stoichiometry (as the charge of the SCI unit in alkaline solution should be −2, the PE–S complex should have a zero net charge at $\beta = 2$). However, since the ζ-potential value reflects the surface charge of the nanoparticles rather than their overall charge, this difference can be explained by the assumption that the charge ratio is shifted in favour of positive charges close to the surface of the aggregates as compared with their inner parts, most probably due to adsorption of excess surfactant cations. Another factor which can influence the charge balance in the system is the possible suppression of the ionization of carboxylic protons in the neighbourhood of SO_3^- groups, so that the effective charge per one SCI unit is lower than −2.

The presence of stable nanoparticles with zero ζ-potential in the PSCI-PEO–HFDPCl system indicates that the particles are not stabilized electrostatically and that a steric stabilization takes place, suggesting that PEO blocks segregate from the insoluble PE–S complex and the nanoparticles have a core–shell structure.

For $\beta > 0.71$, the gyration radius increases again, suggesting that the compact nanoparticles are disrupted and looser aggregates are formed again. This assumption is further supported (i)

by the dependence of $I(0)$, which decreases slightly with increasing β above $\beta = 1.07$, and (ii) by the ζ-potential dependence, which shows that the aggregates overcharge, so that increasing electrostatic repulsion may contribute to the disruption of the nanoparticles and the formation of loose aggregates.

Fig. 3a shows the distributions of the apparent hydrodynamic radii of the aggregates present in PSCI-PEO–HFDPCl solutions at different compositions of the PE–S complexes. In pure PSCI-PEO and at $\beta = 0.18$, the distributions are very broad, indicating the formation of polydisperse aggregates. At $\beta = 0.36$, the distribution becomes clearly bimodal due to the coexistence of larger, loose aggregates with smaller, compact particles with a narrower size distribution which are formed as a result of charge neutralization. The scattering from the latter particles predominates at $\beta = 0.71$, where the minimum of R_H^{app} is also reached at the same point as the minimum R_g and the zero ζ-potential. For higher β, the width of the R_H^{app} distribution is further increased, indicating the disruption of the nanoparticles.

In order to study the influence of screening of electrostatic interactions in the solution on the stability of the formed nanoparticles, we carried out DLS measurements of the PSCI-PEO–HFDPCl system at $\beta = 0.71$ at various concentrations of added NaCl (Fig. 3b). With increasing salt concentration, the DLS size distributions become broader and bimodal, which proves that, at the elevated ionic strength, disruption of the compact particles due to the screening effect occurs, leading to the formation of both smaller copolymer aggregates as well as very large, loose ones with a size similar to those present in the pure PSCI-PEO solution.

3.2 SAXS study of PE–S aggregates structure

In order to obtain information about the structure of aggregates and particles formed in the PSCI-PEO–HFDPCl mixed system, we performed small-angle X-ray scattering experiments. Fig. 4 depicts SAXS data for the stoichiometries of the PE–S corresponding to the pure PSCI-PEO solution ($\beta = 0$), to loose aggregates prior to the formation of insoluble PE–S ($\beta = 0.36$), to compact PE–S nanoparticles ($\beta = 0.71$) and to loose aggregates formed by disruption of compact PE–S nanoparticles in excess of HFDPCl ($\beta = 1.43$).

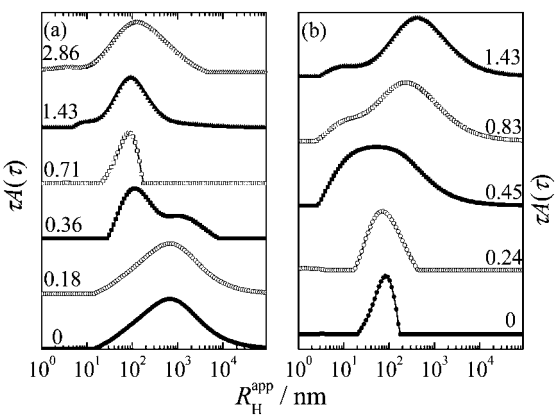

Fig. 3 DLS distributions of apparent hydrodynamic radii at the scattering angle, $\theta = 90°$, for PSCI-PEO–HFDPCl aggregates (a) for various stoichiometric ratios, β, and (b) at $\beta = 0.71$ for various concentrations of added NaCl. The β and c_{NaCl} (in mol L^{-1}) values are given above the corresponding curves.

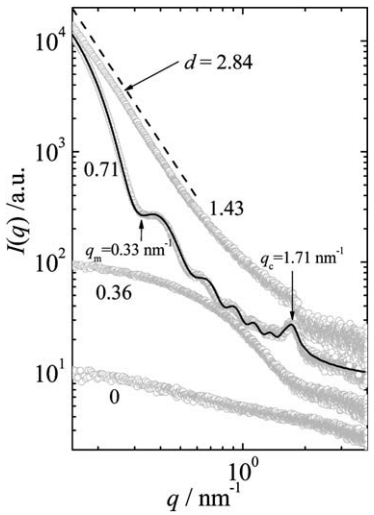

Fig. 4 SAXS of PSCI-PEO–HFDPCl aggregates. The stoichiometric ratios, β, are given next to the corresponding curves. The solid line is the fit of eqn (3) to the data for $\beta = 0.71$; the dashed line is a function proportional to $q^{-2.84}$.

While scattering from PSCI-PEO coils in the pure copolymer solution is too weak for analysis of the curve, after addition of the surfactant, a dominant Guinier scattering contribution with the gyration radius $R_g = 2.04 \pm 0.10$ nm appears for $\beta = 0.36$. This behaviour can be attributed to the formation of spherical HFDPCl micelles attached to PSCI chains.

A large increase in the scattering intensity in the low q range after increasing β from 0.36 to 0.71 corresponds to the formation of large compact PE–S nanoparticles. The scattering curve for the compact particles at $\beta = 0.71$ (the minimum size, zero ζ-potential) exhibits oscillations characteristic for compact scatterers with spherical or cylindrical symmetry, suggesting the formation of spherical or wormlike core–shell particles. The positions of local maxima and minima of the form factors for spheres and cylinders are associated with the radii of the objects, R; for the first minimum, q_m, $q_m R = 4.46$ for the monodisperse spheres and $q_m R = 3.83$ for the long monodisperse cylinders. In the measured scattering curve, $q_m = 0.33$ nm^{-1}, which would correspond to a radius of 13.5 nm for the spherical geometry and 11.6 nm for the cylindrical geometry. The assumption that the PE–S complex forms a compact self-assembly is supported by the scattering behaviour in the high q-range which reflects close packing of the surfactant micelles in the formed PE–S complex, whose characteristic spacing l manifests itself as a structure peak with a maximum at $q_c = 2\pi/l$ (the presence of similar peaks was reported for several other PE–S systems, both in the bulk[6] and in the cores of DHBE core–shell nanoparticles[10,11]). In Section 3.4, we propose a model for the scattering behaviour of the PSCI-PEO–HFDPCl system at $\beta = 0.71$, consistent with the results of Cryo-TEM measurements (Section 3.3).

With a further increase in the amount of surfactant, the oscillations disappear, indicating a loss of the spherical or cylindrical shape. At $\beta = 1.43$, the scattering curve exhibits

a power law behavior, $I(q) \approx q^{-d}$, with the exponent $d = 2.84$ in the q range 0.15–0.4 nm^{-1} corresponding to mass fractal aggregates of a sponge-like structure with the fractal dimension 2.84 on a length scale of approx. 15–40 nm. It is worth mentioning that the SAXS curve for the fractal aggregate retains the structure peak at $q = 1.71$ nm^{-1}, which means that the packing of surfactant micelles in the aggregate is preserved, even though the broadening of the peak indicates that the correlation length within the packed complex of HFDPCl micelles and PSCI chains is decreased compared with the compact particles at $\beta = 0.71$.

3.3 Cryo-TEM and AFM imaging of PE–S aggregates

Since SAXS measurements indicated that, at the stoichiometric ratio $\beta = 0.71$, PSCI-PEO and HFDPCl co-assemble in spherical and/or cylindrical nanoparticles, the PSCI-PEO–HFDPCl system of this composition was imaged by Cryo-TEM and AFM. Cryo-TEM (Fig. 5a; for zoomed views, see Fig. S1 in the ESI†) shows (i) wormlike nanoparticles with a cross-sectional radius of about 13 nm and a length of several hundreds of nm and (ii) spherical objects with a similar radius as the cross-sectional radius of the wormlike particles, which can either be spherical particles or short cylindrical particles imaged along their longitudinal axes. The presence of elongated particles can be explained by the fact that HFDPCl undergoes a transition from spherical to threadlike micelles,[23] which, occurring simultaneously with the co-assembly of the surfactant cations with PSCI blocks, can lead to the formation of wormlike core–shell PE–S particles. (A few isolated threadlike HFDPCl micelles can also be observed in the PSCI-PEO–HFDPCl system at $\beta = 0.71$. A zoom of a Cryo-TEM micrograph showing such a micelle is shown in Fig. S1 in the ESI†.)

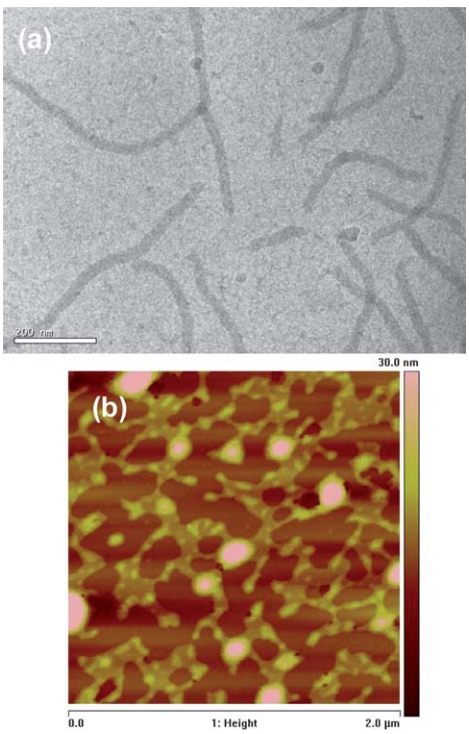

Fig. 5 Images of PSCI-PEO–HFDPCl nanoparticles at the stoichiometric ratio, $\beta = 0.71$: (a) Cryo-TEM (scale bar = 200 nm), (b) AFM (2 × 2 µm^2 scan).

Fig. 5b is an AFM scan of PE–S nanoparticles at $\beta = 0.71$ in the dry state, deposited on a mica surface from a diluted aqueous solution ($c = 10^{-2}$ mg mL^{-1}). Instead of isolated clusters, interconnected particles form a continuous two-dimensional network with both variable height and width on the substrate surface. It is noteworthy that the minimum width of the network is about 30 nm, which is in accordance with the dimensions of the worms. This observation suggests that, at these points, the junctions of the network are formed by single wormlike nanoparticles.

3.4 SAXS model for compact nanoparticles

In order to describe the SAXS scattering behaviour of the PEO–HFDPCl system at $\beta = 0.71$, we have taken into account the Cryo-TEM results which show that, at this stoichiometric ratio, the PE–S complex forms both wormlike and spherical (or short cylindrical) particles. In the proposed model, scattering from wormlike micelles, $P_{\mathrm{worm}}(q,L,b,R_c)$, is described by the form factor for the semiflexible chain with the contour length L and the Kuhn length b,[32] assuming that the chain has a local cylindrical morphology with homogeneous scattering length density and cross-sectional radius R_c, while spherical particles are treated by the simple form factor $P_{\mathrm{sphere}}(q,R_s)$ for monodisperse spheres with radius R_s.

In addition to the scattering contributions from worms and spheres, it was necessary to treat correlations in the high q region. The latter contribution was modelled by the structure factor for disordered cell–cell correlations,[33] $S_{\mathrm{cor}}(q,l,\xi)$, where ξ is the correlation length. The overall scattering function, $I_{\mathrm{PE-S}}(q)$, thus has the form,

$$I_{\mathrm{PE-S}}(q) = I_1 P_{\mathrm{worm}}(q,L,b,R_c) + I_2 P_{\mathrm{sphere}}(q,R_s) + I_3 S_{\mathrm{cor}}(q,l,\xi) \quad (3)$$

where I_1 and I_2 are the forward scattering intensities for worms and spheres, respectively, and I_3 is the amplitude of the correlation peak. (The full expression for $I_{\mathrm{PE-S}}(q)$ is in the ESI†.)

The resulting parameters of the fit of eqn (3) to the SAXS data for $\beta = 0.71$ (shown in Fig. 4 as the solid line) with fixed contour length $L = 600$ nm and Kuhn length $b = 200$ nm are $R_c = 15.5 \pm 0.2$ nm, $R_s = 13.8 \pm 0.1$ nm, $l = 3.67 \pm 0.02$ nm and $\xi = 6.8 \pm 0.5$ nm, with $\chi^2 = 5.4$. The radii of the worms and spheres are consistent with the Cryo-TEM images, being only slightly larger than those obtained from the microscopic image. This difference can be ascribed to the fact that hydrated aggregates or domains in the particles are not visible because of a low electron contrast difference between these structures and the amorphous ice of the solvent. The characteristic packing distance is comparable with the cross-sectional diameter of threadlike micelles. It should also be pointed out that even though the scattering contribution from the spheres is relatively low ($I_2/I_1 = 1.7 \times 10^{-2}$), it cannot be neglected as running the fit with the I_2 value fixed at $I_2 = 0$ (without the presence of spherical particles) results in a significantly higher χ^2 value ($\chi^2 = 62.4$), so that the SAXS data analysis corroborates the Cryo/TEM observation of spherical particles coexisting with the worms.

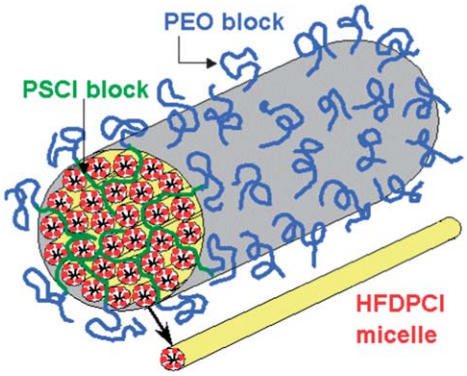

Fig. 6 Scheme of the PSCI-PEO–HFDPCl core–shell wormlike nanoparticle.

4 Conclusion

In this article, we have studied the interaction of a double hydrophilic anionic block polyelectrolyte, PSCI-PEO, with a cationic fluorosurfactant, HFDPCl, in aqueous solutions, by a combination of scattering (SLS, DLS, SAXS) and microscopic (Cryo-TEM, AFM) techniques. We have demonstrated that double hydrophilic block polyelectrolytes are able to form PE–S complexes with oppositely charged fluorosurfactants in a similar way as for PE–S complexes involving hydrocarbon ionic surfactants, so that at a stoichiometric ratio between SCI units and HFDPCl corresponding to ζ-potential values of the aggregates close to zero, the block polyelectrolyte co-assembles with the fluorosurfactant in compact core–shell nanoparticles with the core formed by the phase consisting of densely packed fluorosurfactant micelles and polyelectrolyte blocks and the shell of hydrophilic neutral blocks. In the PSCI-PEO–HFDPCl system, however, micellization of HFDPCl in threadlike, cylindrical micelles causes the formation of long wormlike core–shell nanoparticles (coexisting with a small fraction of spherical PE–S nanoparticles), as was shown by cryogenic transmission electron microscopy and attested by SAXS measurements. The formed core–shell nanoparticles are apt to disruption if HFDPCl is added in excess with respect to the stoichiometry corresponding to the zero effective charge.

SAXS data for the wormlike core–shell nanoparticles were treated by the model for semiflexible chains with the local cylindrical cross-section and homogeneous scattering length density, with an additional term taking into account the correlations between densely packed surfactant micelles in the core of the nanoparticles. The structure of the wormlike nanoparticles proposed on the basis of SAXS and Cryo-TEM measurements is depicted in Fig. 6.

Acknowledgements

The authors acknowledge the financial support from the Ministry of Education of the Czech Republic (long-term research project no. MSM0021620857), Czech Science Foundation grants P208/10/0353 (M.Š.), P208/10/1600 (B.A.), P208/12/P236 (M.U.) and P302/12/G157 (L.K.) and Charles University grant UNCE204022 (L.K.). The authors wish to thank Dr M. Urbanová of the Institute of Macromolecular Chemistry of the Academy of Sciences of the Czech Republic for sample characterization by ^{13}C solid state NMR. B.A. acknowledges the kind technical support from Manfred Rössle at the Petra III BioSAXS beamline.

Notes and references

1 I. K. Voets, A. de Keizer and M. A. CohenStuart, *Adv. Colloid Interface Sci.*, 2009, **147–148**, 300.
2 D. Langevin, *Adv. Colloid Interface Sci.*, 2009, **147–148**, 170.
3 S. Zhou and B. Chu, *Adv. Mater.*, 2000, **12**, 545.
4 D. Chu and J. K. Thomas, *J. Am. Chem. Soc.*, 1986, **108**, 6270.
5 P. Hansson, *Langmuir*, 2001, **17**, 4167.
6 K. Kogej, *J. Phys. Chem. B*, 2003, **107**, 8003.
7 A. V. Kabanov, T. K. Bronich, V. A. Kabanov, K. Yu and A. Eisenberg, *J. Am. Chem. Soc.*, 1998, **120**, 9941.
8 T. K. Bronich, A. M. Popov, A. Eisenberg, V. A. Kabanov and A. V. Kabanov, *Langmuir*, 2000, **16**, 481.
9 T. K. Bronich, A. V. Kabanov, V. A. Kabanov, K. Yu and A. Eisenberg, *Macromolecules*, 1997, **30**, 3519.
10 J.-F. Berret, G. Cristobal, P. Hervé, J. Oberdisse and I. Grillo, *Eur. Phys. J. E*, 2002, **9**, 301.
11 J.-F. Berret, B. Vigolo, R. Eng, P. Hervé, I. Grillo and L. Yang, *Macromolecules*, 2004, **37**, 4922.
12 J. Courtois and J.-F. Berret, *Langmuir*, 2010, **26**, 11750.
13 K. Matsuoka and Y. Moroi, *Curr. Opin. Colloid Interface Sci.*, 2003, **8**, 227.
14 A. F. Thünemann, *Langmuir*, 1998, **14**, 4898.
15 C. K. Ober and G. Wegner, *Adv. Mater.*, 1997, **9**, 17.
16 A. F. Thünemann and K. H. Lochhaas, *Langmuir*, 1999, **15**, 6724.
17 A. F. Thünemann, *Prog. Polym. Sci.*, 2002, **27**, 1473.
18 S.-S. Hou, J.-K. Tzeng and M.-H. Chuang, *Soft Matter*, 2010, **6**, 409.
19 H. Peng, D. Chen and M. Jiang, *J. Phys. Chem. B*, 2003, **107**, 12461.
20 Z. Hu, W. Verheijen, J. Hofkens, A. M. Jonas and J.-F. Gohy, *Langmuir*, 2007, **23**, 116.
21 A. Laschewsky, M. Mertoglu, S. Kubowicz and A. F. Thünemann, *Macromolecules*, 2006, **39**, 9337.
22 S. Pispas, *J. Polym. Sci., Part A: Polym. Chem.*, 2006, **44**, 606.
23 K. Wang, G. Karlsson, M. Almgren and T. Asakawa, *J. Phys. Chem. B*, 1999, **103**, 9237.
24 M. Uchman, M. Štěpánek, K. Procházka, G. Mountrichas, S. Pispas, M. Špírková and A. Walther, *Langmuir*, 2008, **24**, 12017.
25 M. Uchman, M. Štěpánek, K. Procházka, G. Mountrichas, S. Pispas, I. K. Voets and A. Walther, *Macromolecules*, 2009, **42**, 5605.
26 S. Pispas, *J. Phys. Chem. B*, 2007, **111**, 8351.
27 S. Pispas, *Soft Matter*, 2011, **7**, 474.
28 M. Karayianni, S. Pispas, G. D. Chryssikos, V. Gionis, S. Giatrellis and G. Nounesis, *Biomacromolecules*, 2011, **12**, 1697.
29 M. Uchman, K. Procházka, K. Gatsouli, S. Pispas and M. Špírková, *Colloid Polym. Sci.*, 2011, **289**, 1045.
30 T. Asakava, H. Hisamatsu and S. Miyagishi, *Langmuir*, 1995, **11**, 478.
31 J. Dubochet, M. Adrian, J. J. Chang, J. C. Homo, J. Lepault, A. W. McDowall and P. Q. Schultz, *Annu. Rev. Biophys. Biomol. Struct.*, 1988, **21**, 129.
32 J. S. Pedersen and P. Schurtenberger, *Macromolecules*, 1996, **29**, 7602.
33 N. Lei, C. R. Safinya, D. Roux and K. S. Liang, *Phys. Rev. E: Stat. Phys., Plasmas, Fluids, Relat. Interdiscip. Top.*, 1997, **56**, 608.